

Global full- f gyrokinetic simulations of plasma turbulence

V. Grandgirard¹, Y. Sarazin¹, P. Angelino¹, A. Bottino², N. Crouseilles³, G. Darmet¹, G. Dif-Pradalier¹, X. Garbet¹, Ph. Ghendrih¹, S. Jolliet⁵, G. Latu⁴, E. Sonnendrücker³, L. Villard⁵

¹ CEA/DSM/DRFC, Association Euratom-CEA, Cadarache, 13108 St Paul-lez-Durance, France.

² Max Plank Institut für Plasmaphysik, IPP-EURATOM Association Garching, Germany.

³ IRMA, Université Louis Pasteur, 7, rue René Descartes, 67084 Strasbourg Cedex, France.

⁴ LaBRI, 341 cours Libération, 33405 Talence Cedex, France.

⁵ CRPP, Association Euratom-Confédération Suisse, EPFL, 1015 Lausanne, Switzerland.

E-mail: virginie.grandgirard@cea.fr

Abstract. Critical physical issues can be specifically tackled with the global full- f gyrokinetic code GYSELA. Four main results are presented. First, the validity of simulating a fraction of torus is shown to increase with decreasing ρ_* . Second, the self consistent treatment of the equilibrium and fluctuations highlights the competition between two compensation mechanisms for the curvature driven vertical charge separation, namely parallel flow and polarization. The impact of the latter on the turbulent transport is discussed. Third, the transport scaling with ρ_* is found to depend both on ρ_* itself and on the distance to the linear threshold. Finally, a statistical steady-state turbulent regime is achieved in a reduced version of GYSELA by prescribing a constant heat source.

PACS numbers: 52.65.Tt, 52.30.Gz

Submitted to: *Plasma Phys. Control. Fusion*

1. Introduction

Gyrokinetic codes are now mature enough to address experimentally relevant pieces of physics [1, 2, 3, 4]. In this framework, global and full- f codes allow one to specifically address physical issues of outermost importance in fusion devices. Due to their huge demands in terms of both numerical memory and CPU time consumption, such full- f simulations have become possible only very recently. On the one hand, simulating a whole part of the tokamak cross-section allows one to capture large scale transport

events, eventually leading to non-local transport and turbulence spreading. Especially, such processes can bring new ingredients into the physics governing scaling laws. On the other hand, full- f codes solve self-consistently the equilibrium and the fluctuations, without any scale separation assumption. In this case, properly defining the gyrokinetic equilibrium reveals crucial to discriminate between instability driven fluctuations and time evolution towards the equilibrium. Besides, non-equilibrium initial states can also impact the turbulence dynamics itself. Finally, full- f codes open the route towards more realistic flux-driven models, where the turbulence drive is no longer ensured by a prescribed gradient or fixed thermal baths at the boundaries, but by an incoming heat and/or particle source such as in the experiments.

The present paper focusses on some of the physical implications of global and full- f gyrokinetic code. The 5D GYSELA (GYrokinetic SEmi-LAgrangian) code is used. It models the Ion Temperature Gradient (ITG) driven turbulence in a simplified toroidal geometry with a Semi-Lagrangian numerical scheme [5]. The model is detailed in section 2. The problem of solving the gyrokinetic equilibrium, especially in full- f codes as GYSELA, is addressed in section 3. As reported earlier [6], the code has already been benchmarked, both linearly and non-linearly against the CYCLONE test case [7]. In section 4, a further validation based on non-linear comparisons with the ORB5 code [8] is presented. In section 5, the effect of reducing the fraction of the torus that is simulated is discussed. Results on the ρ_* scaling of the turbulent transport, ρ_* being the ratio of the ion Larmor radius ρ_i to the minor radius a , are reported in section 6. Consistently with previous works, the correlation time and correlation length are found to be consistent with the gyroBohm, respectively Bohm, scaling at small ρ_* and above the linear threshold, resp. at large ρ_* and close to the threshold. Finally, turbulence in the flux driven regime is investigated with a reduced 3D gyrokinetic model, used as a paradigm, section 7. The bursty character of the dynamics, as well as the departure from the Maxwellian, are reported.

2. Gyrokinetic system solved by Gysela

The model focusses on the turbulent transport driven by the collisionless Ion Temperature Gradient (ITG) driven instability in a simplified toroidal geometry: the magnetic flux surfaces are concentric torii with circular poloidal cross-sections. The magnetic field is $\vec{B} = (B_0 R_0/R) (\vec{e}_\varphi + (r/q R_0)\vec{e}_\theta)$. B_0 and R_0 being the magnetic field and the major radius of the torus computed at the magnetic axis, with $R = R_0 + r \cos \theta$. \vec{e}_θ and \vec{e}_φ are the unit vectors in the two periodic directions, poloidal and toroidal respectively. The safety factor q is given a standard monotonous profile, from $q \approx 1$ in the core towards $q \approx 2.5$ at the edge of the simulation domain. Within the electrostatic approximation, the electric field $\vec{E} = -\vec{\nabla}\phi$, where ϕ is the electric potential. In the low frequency turbulence regime, such that ω is much smaller than the ion cyclotron frequency $\omega_c = e_i B_0/m_i$, the gyrokinetic description is appropriate. v_\parallel is the velocity parallel to the magnetic field, and the magnetic moment $\mu = m_i v_\perp^2/(2B)$ is an adiabatic

invariant. In the code the time evolution of the guiding-center 5D distribution function $\bar{f}(r, \theta, \varphi, v_{\parallel}, \mu, t)$ is governed by the following gyrokinetic equation:

$$\partial_t \bar{f} + (\vec{v}_E + \vec{v}_D) \cdot \vec{\nabla}_{\perp} \bar{f} + (v_{\parallel}/R) \partial_{\varphi} \bar{f} + \dot{v}_{\parallel} \partial_{v_{\parallel}} \bar{f} = 0 \quad (1)$$

with $\vec{\nabla}_{\perp} = (\partial_r, \frac{1}{r} \partial_{\theta})$. $\vec{v}_E = \vec{B} \times \vec{\nabla}(\mathcal{J} \cdot \phi)/B^2$ is the $E \times B$ electric drift velocity. The gyro-average operator \mathcal{J} corresponds to the zero order Bessel function $J_0(k_{\perp} \rho_i)$ in Fourier space, ρ_i being the ion Larmor radius. At low β , the curvature drift velocity is equal to $\vec{v}_D = ((m_i v_{\parallel}^2 + \mu B)/e B^3) \vec{B} \times \vec{\nabla} B$. In the large aspect ratio limit, $m_i \dot{v}_{\parallel} = e_i E_{\parallel} - \mu \nabla_{\parallel} B + m v_{\parallel} \vec{v}_E \cdot \vec{\nabla} B/B$ with $\nabla_{\parallel} = 1/R [\partial_{\varphi} + (1/q(r)) \partial_{\theta}]$. The self-consistency is ensured by the quasi-neutrality constraint:

$$-\frac{1}{n_0(r)} \nabla_{\perp} \cdot \left[\frac{n_0(r)}{B_0 \omega_c} \nabla_{\perp} \phi \right] + \frac{e}{T_e(r)} [\phi - \langle \phi \rangle] = \frac{1}{n_0(r)} [n_{Gi}(r, \theta, \varphi) - n_{Gi_{\text{init}}}(r, \theta)] \quad (2)$$

The polarization term (first term on the left hand side) accounts for the difference between the ion guiding-center density $n_{Gi} = 2\pi B(r, \theta)/m_i \int d\mu \int dv_{\parallel} \mathcal{J} \cdot \bar{f}$ and the particle density. The brackets $\langle \cdot \rangle$ refer to the magnetic flux surface average, i.e. $\langle \cdot \rangle = 1/(2\pi)^2 \int \int \cdot d\theta d\varphi$. The correction term $n_{Gi_{\text{init}}}$ is equal to $n_{Gi_{\text{init}}} = 2\pi B(r, \theta)/m_i \int d\mu \int dv_{\parallel} \mathcal{J} \cdot f_{\text{init}}$ where f_{init} is the initial distribution function. More details on the system are given in [6].

Since the electrons are adiabatic, there is no net particle transport. The radial density profile remains thus constant in time. The distribution function is prescribed to be a Maxwellian at both radial boundaries with two different temperatures. Periodic boundary conditions are applied along θ and φ . The initial condition consists of an initial distribution function f_{init} , which can be a local Maxwellian or a canonical Maxwellian, as discussed in section 3, perturbed by a sum of (m, n) Fourier modes with random phase and prescribed magnitude. Here, m and n are the poloidal and toroidal wave numbers, respectively. The quasi-neutrality equation (2) is solved in Fourier space for the poloidal and toroidal directions, while finite differences are used in the radial direction. The Bessel function of the gyroaverage operator is replaced by a Padé approximation [9]. The gyrokinetic equation (1) is solved with a semi-lagrangian scheme [10]. Such a method has proven to be powerful in a 4D version of the code, focusing on the slab branch of the ITG turbulence in the drift-kinetic limit [5]. Significant effort has been devoted to improving the code parallelization [11, 12], that is especially difficult for Eulerian-like numerical schemes. The present version exhibits an efficacy of about 70% on 1024 processors.

3. Non linear simulations with a global full- f code

Several publications [13, 14] have stressed the importance of initializing gyrokinetic simulations with a well-defined equilibrium. In the absence of collisions, an equilibrium distribution function fulfills $[H_{\text{eq}}, f_{\text{eq}}] = 0$, with $[\cdot, \cdot]$ the Poisson bracket. The equilibrium gyrokinetic Hamiltonian H_{eq} depends on the motion invariants only, namely the energy \mathcal{E} , the magnetic moment μ and the toroidal momentum P_{φ} . Consequently,

any function of \mathcal{E} , μ and P_φ will satisfy the equilibrium conditions. A convenient form is provided by a local Maxwellian where the radius is replaced by an effective radial coordinate \bar{r} function of the invariants [15, 16]. This corresponds to the so-called *canonical Maxwellian* initialization f_{CM} . In such an equilibrium, the curvature drift which induces a vertical charge polarization is compensated by the ion parallel flow. This flow, analogous to the Pfirsch-Schlüter current carried by the electrons, naturally emerges from the v_\parallel dependence of P_φ . Indeed, the distribution function f_{CM} is *not even in v_\parallel* unlike standard local Maxwellian f_{LM} . For the latter distribution function, there is no parallel flow and the charge separation gives rise to a large scale electric field. In this case, the charge separation tends to being compensated by a polarization flow. The early dynamics of the resulting electric potential ϕ can be easily recovered analytically [17]. At leading order, it is governed by the curvature drift. Especially, it is found that $\phi \approx \phi_{00} + \phi_{10}^s \sin \theta + \phi_{10}^c \cos \theta$, with $e\phi_{00}/T_0 \propto \rho_*^2 (\omega_c t)^2$ and $e\phi_{10}^s/T_0 \propto \rho_*^2 \omega_c t$, consistently with the numerical simulations. It should be noticed that such a ρ_*^2 dependence does not mean that these flows remain weak at small ρ_* values. Indeed, an upper boundary of the time duration of the growth of these flows is given by the time at which the parallel dynamics enters into play to counterbalance the charge polarization. In the end, the saturation level of these polarization flows is significant, and of the order of a few tenth of T_0/e . Conversely, the cosine component ϕ_{10}^c is orders of magnitude smaller. The $\sin \theta$ component ϕ_{10}^s grows first, linearly in time, as a result of the up-down asymmetry of the curvature drift. The oscillatory behavior at the GAM (Geodesic Acoustic Mode) frequency is recovered at later times, when the $E \times B$ drift is no longer negligible and enters the dynamics.

An interesting question is whether such sheared flows, which result from the re-arrangement of non-equilibrium initialization, can durably prevent the onset of turbulence. In this framework, two simulations at $\rho_* = 5.10^{-3}$ and with the same initial temperature gradient – well above the threshold – are compared. They only differ by their initial distribution function, either canonical or Maxwellian. The time evolution of the heat diffusivity is plotted on figure 1 for the two cases. The turbulent transport is clearly delayed when starting from an initial local Maxwellian, by about $1500 \omega_c^{-1}$ in this case. As seen on the upper panel of figure 1, the effective growth rate is reduced for the local Maxwellian (from $\gamma_{\text{CM}} \approx 2.3 \cdot 10^{-3} \omega_c$ to $\gamma_{\text{LM}} \approx 1.5 \cdot 10^{-3} \omega_c$), when sheared flows are present. Such a picture is in qualitative agreement with a reduction of the effective linear growth rate by the shearing rate. Also, the turbulence overshoot at the end of the linear phase is smeared out. However, both simulations yield similar diffusivities in the turbulent regime, as exemplified by the values at the end of the simulations, see figure 1.

4. Non-linear benchmarks with ORB5 code

The GYSELA code has been benchmarked against the CYCLONE test case [7], both linearly and non-linearly, as reported earlier [6]. Also, the now standard test of poloidal

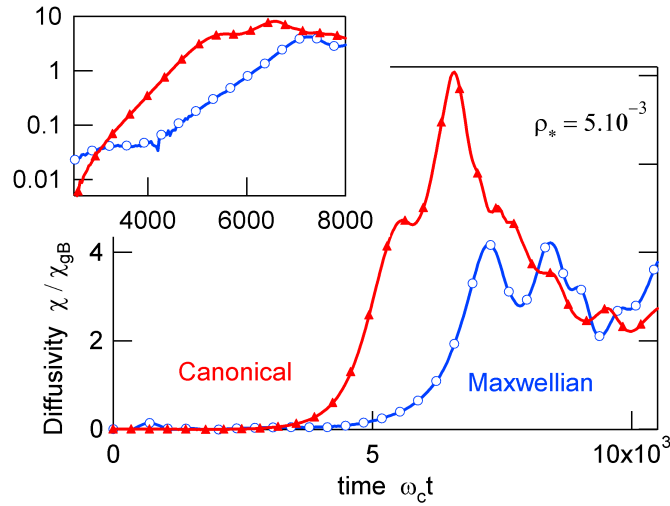


Figure 1. (Color online) Time evolution of the turbulent diffusivity χ_{\perp} ($\rho_* = 1/200$) when initializing the distribution function with a canonical equilibrium or a local Maxwellian. Top panel: zoom in log-lin scale.

flow screening in the collisionless regime [18] has been performed successfully. Here, we report first results of the non-linear comparison with the ORB5 code [8]. Both codes are global, and model the same gyrokinetic equations. However, ORB5 uses a completely different numerical scheme. It is a δf Particle in Cell (PIC) scheme, where the perturbed part of the distribution function, $\delta f = f - f_{\text{init}}$, is sampled by a random distribution of markers, according to the MonteCarlo method. The positions of the markers are evolved in time following the characteristics of the gyrokinetic equation (Lagrangian method). The time evolution uses a 4th order Runge-Kutta scheme and the quasi-neutrality equation is solved with a 3D Finite Element Method (FEM). The gyroaverage is approximated by an adaptive numerical average. Another difference resides in the zonal flow term $\bar{\phi}$ which is approximated by ϕ_{00} in GYSELA, while the full geometric coupling is kept in ORB5. Finally, the right hand side of the quasi-neutrality equation is Fourier filtered along the magnetic field lines ($m = nq(s) \pm \Delta m$) in ORB5. This filter allows one to reduce the statistical noise associated with the PIC discretization by filtering out the nonphysical high k_{\parallel} modes [19].

The parameters for the benchmark are based on the CYCLONE test case [7]. The minor radius is $a = 0.625$ m, the inverse aspect ratio is $\varepsilon = a/R = 0.36$. The magnetic field on axis is $B_0 = 1.91$ T. The safety factor profile is given by $q(r) = 0.854 + 2.184(r/a)^2$. The initial temperature gradients are given by $d \log / dr = -L_T^{-1} [-1 + \cosh^{-2}((r - 0.1a)/0.04) + \cosh^{-2}((r - 0.9a)/0.04)]$ with the conditions $T_e(r/a = 0.5) = T_i(r/a = 0.5) = 2$ KeV. The ratio of the temperature characteristic length over the density one is: $L_T/L_n = 0.21$. Notice that the mean temperature profile is not frozen. As a result of the turbulent heat flux, the temperature gradient decreases with time. The boundary conditions are somewhat different in both

codes: while temperature is kept constant at both radial boundaries in GYSELA, leading to steep gradients within thin boundary layers, the core boundary temperature is free to evolve in ORB5, leading to a so-called decaying turbulence regime.

The two simulations have been performed at $\rho_* = 1/184.7$. GYSELA was run with about 1 billion grid points in the 5D phase space, while ORB5 used about 33 millions of grid points in space with 256 millions of pseudo-particles. Both simulations ran approximatively 36 hours on 128 processors, using machines of similar performances. The time evolution of the diffusivity χ , normalized by the gyro-Bohm diffusivity $\chi_{gB} = \rho_s^2 c_s / L_n$, and of the normalized temperature gradient R_0 / L_T are plotted on figure 2 for both codes. Both quantities are averaged over flux surfaces, as well as over the radial interval $0.4 \leq r/a \leq 0.6$. Time has been shifted by approximately $-7.10^3 \omega_c^{-1}$ for the ORB5 simulation so as to account for the longer transient at the beginning in this code. First, one observes that both codes, GYSELA and ORB5, yield the same level of turbulent transport in the non-linear regime. Also, such magnitudes of χ are in agreement with those reported in other gyrokinetic simulations [7]. Second, the temperature profile relaxes faster in ORB5 than in GYSELA. Such a difference could result from the difference in the boundary conditions. Indeed, while the whole profile is allowed to freely evolve in ORB5, the temperature is kept constant at both radial boundaries in GYSELA. Also note that, at a given value of R_0 / L_T , ORB5 predicts a larger transport than GYSELA. Such a mismatch could arise from the intrinsic difference between full- f and δf schemes. Indeed, as discussed in section 3, the equilibrium electric field is self-consistently computed in GYSELA. This likely leads to a larger magnitude of the zonal component ϕ_{00} and of the resulting poloidal velocity shear in GYSELA, eventually reducing the level of turbulent transport. This benchmark will be further detailed in a future publication.

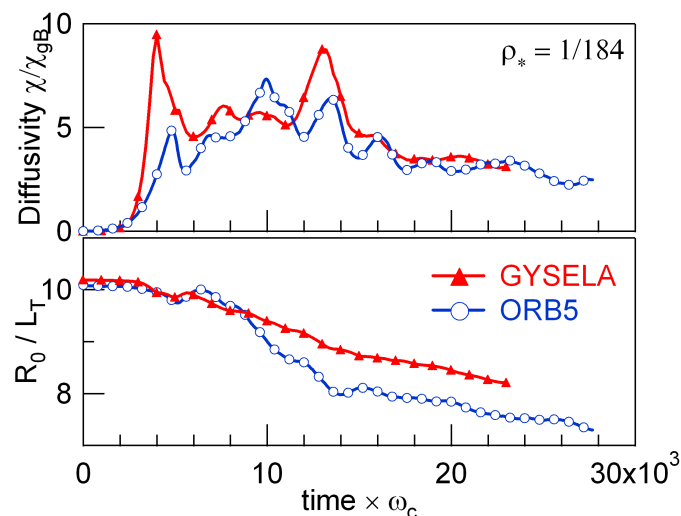


Figure 2. (Color online) Time evolution of the turbulent diffusivity χ_{\perp} (top) and of the normalized temperature gradient (bottom) in GYSELA and ORB5 for $\rho_* = 1/184.7$.

5. Validity of simulations on a fraction of torus

With the aim of reducing the large numerical resources required by such a global full- f code, attempts to run on fractions of torus have been performed, with the toroidal extent equal to $L_\varphi = 2\pi/p$ ($p \in \mathbb{N}$). The code is such that periodicity is always imposed along the toroidal direction, whatever L_φ . Consequently, only those toroidal n modes proportional to p are accessible for a fraction $L_\varphi = 2\pi/p$: $n = \{0, p, 2p, 3p, \dots, N\}$. Conversely, all poloidal m modes are retained. Four simulations have been performed at $\rho_* = 1/128$: $L_\varphi = 2\pi/p$, with $p = 2, 4, 8$ and 16 . For each case, the corresponding mesh is equal to $(r, \theta, \varphi, v_\parallel, \mu) = (128, 256, 128/p, 32, 8)$. In this case, each simulation exhibits the same ratio of resonant modes with respect to the total number of modes (m, n) . For a given value of the temperature gradient $\nabla_\perp T/T$, the number of linearly unstable modes scales like $(\rho_* p)^{-1}$. As a result, the smaller ρ_* , the larger p can be while allowing one to trigger the same number of unstable modes. Since the turbulent regime requires a sufficient number of unstable modes to reach saturation, simulations at small ρ_* should still be accurate at small fraction of torus (large p).

The time evolution of the diffusivity is plotted on figure 3. There is some hint of departure from the average magnitude of χ for the $L_\varphi = 2\pi/16$ case that exhibits a slightly smaller diffusivity. When comparing the correlation time and the radial correlation length of the electric potential fluctuations $\delta\phi = \phi - \langle\phi\rangle$, a more pronounced difference can be observed, figure 4. The Eulerian self-correlation function is defined as $C_{\delta\phi}(\Delta r) = \int d\Gamma \delta\phi(\mathbf{r}, \theta, t) \delta\phi(\mathbf{r} + \Delta\mathbf{r}, \theta, t) / \int d\Gamma |\delta\phi(\mathbf{r}, \theta, t)|^2$, with $\int d\Gamma \equiv \int_{t_0}^{t_0+\tau} \frac{dt}{\tau} \int_0^{2\pi} \frac{d\theta}{2\pi} \int_{r_0}^{r_0+L} \frac{dr}{L}$. The radial window typically covers the central 40% of the radial domain. A similar definition is used for $C_{\delta\phi}(\Delta t)$. In figure 4, the reference time $t_0 = 10000/\omega_c$ is in the turbulent phase and $\tau = 7500/\omega_c$. Clearly, the most poorly discretized case $L_\varphi = 2\pi/16$ exhibits a different shape for both $C_{\delta\phi}(\Delta r)$ and $C_{\delta\phi}(\Delta t)$. In particular, a significant correlation still exists at large distances and at long time duration. The correlation is equal to 0.2 for $\Delta r \approx 17\rho_i$ and $\Delta t \approx 3000\omega_c^{-1}$. Such values are consistent with the fact that, with such a small number of linearly unstable modes (about 2), the system remains close to the linear regime and is dominated by the physics of global modes. With a larger fraction of the torus $L_\varphi \geq 2\pi/8$, the number of linearly unstable modes appears to be large enough to lead to comparable physics in terms of the transport coefficients and correlation time and distance.

6. Transport scaling with ρ_*

The kinetic equation exhibits scale invariance properties [20]. As a consequence, the energy confinement time τ_E is expected to be governed by a set of key dimensionless parameters. A key quantity is the ρ_* parameter. Indeed, present experimental devices cannot access the small ρ_* values expected in ITER, of the order of $2 \cdot 10^{-3}$, while in the JET tokamak the most performing discharges have 2 to 3 times larger ρ_* . Furthermore, in the empirical scaling laws of τ_E , the power exponent of ρ_* is the largest, namely

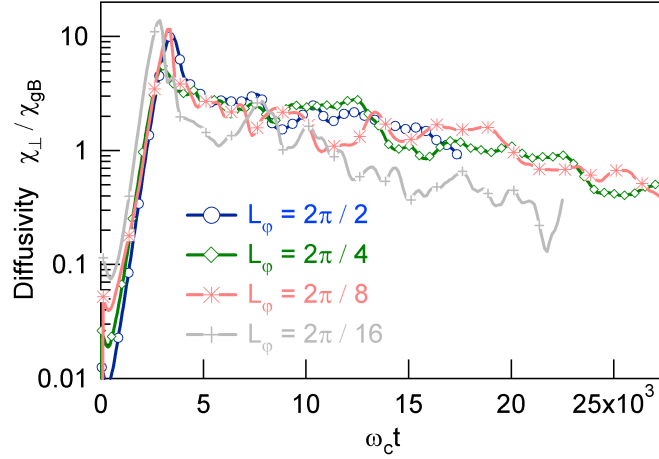


Figure 3. (Color online) Time evolution of the diffusivity for four simulations with different toroidal lengths L_φ .

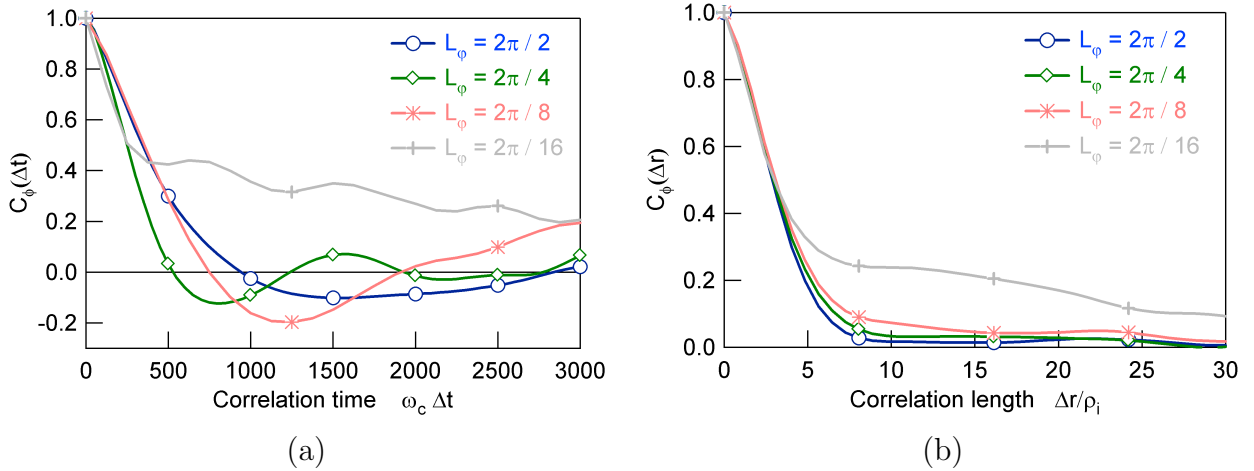


Figure 4. (Color online) (a) Temporal self-correlation function $C_{\delta\phi}(\Delta t)$ and (b) Radial self-correlation function $C_{\delta\phi}(\Delta r)$, for four values of L_φ .

$\omega_c \tau_E \propto \rho_*^{-2.8}$, with ω_c the cyclotron frequency. Such a power law is consistent with the so-called gyroBohm scaling ($\chi_\perp \approx \rho_* \chi_B$ and $\chi_B = \rho_i^2 \omega_c$), so that $\omega_c \tau_E \approx \omega_c a^2 / \chi_\perp \propto \rho_*^{-3}$. After the pioneering works using fluid models to investigate this critical issue [21], two recent gyro-kinetic simulations [1, 22] report a transition from Bohm to gyro-Bohm scaling when ρ_* decreases towards ITER-like values. Two open issues remain: what is the ρ_* value of this transition and what is the physical mechanism? So far, two main explanations have been proposed. On the one hand, shear flow stabilization leading to $\chi_\perp \approx \rho_* \chi_B (1 - \alpha \rho_*)$ [23]. This results from the scaling of the $E \times B$ shearing rate like $\gamma_E \approx \rho_* \gamma_{lin}$, with $\gamma_{lin} \approx (k_\theta \rho_i) c_s / (RL_T)^{1/2}$ the linear growth rate of the instability in the absence of shear flow. On the other hand, large scale transport events can lead to large correlation lengths of the form $\lambda_c \approx (a \rho_i)^{1/2}$. In this case, non diffusive transport

or turbulence spreading are expected to be at work. Surprisingly, the latter mechanism leads to the same type of scaling for the diffusivity, namely $\chi_{\perp} \approx \rho_* \chi_B / (1 + \alpha \rho_*)$ [24]. It is worth noticing that such a physics can only be addressed with global codes.

A scan in ρ_* values has been performed with the global full- f code GYSELA to study this question. Three values have been analyzed, ranging from large ($\rho_* = 2.10^{-2}$) to intermediate ($\rho_* = 10^{-2}$ and $\rho_* = 5.10^{-3}$) values. Since the equilibrium is allowed to evolve in GYSELA, the mean temperature profile tends to relax towards the threshold (at $R/L_T \approx 6$) in the turbulent regime. Such dynamics are apparent on figure 5. The dotted line refers to the best fit of the Lawrence Livermore National Laboratory results (flux-tube PIC code) for the CYCLONE case, as discussed in reference [7]. Also, the three cases do not start from the same temperature gradient. This results from the difficulty in matching radial profiles at different ρ_* , when initializing with a canonical distribution function [15] (see section 3). The correlation length and time of the electric

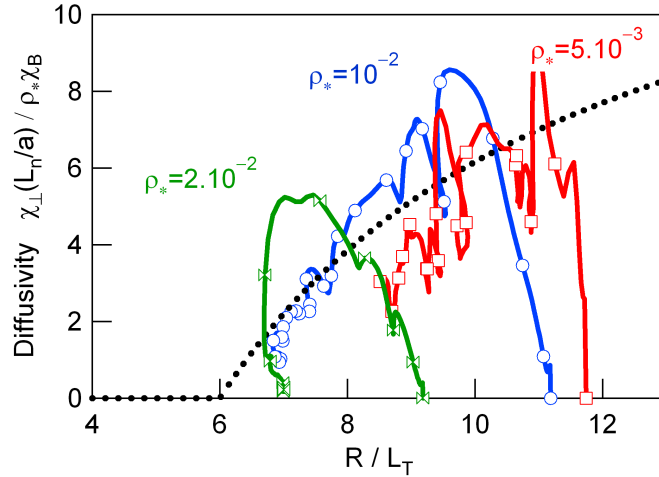


Figure 5. (Color online) Time evolution of the turbulent diffusivity χ_{\perp} as a function of the normalized temperature gradient for three values of ρ_* .

potential fluctuations are presented on figures 6 and 7, for two different choices of t_0 : either when the system is still well above the threshold (figures 6 (a) and (b)), *i.e.* rather early in the simulation, or close to the threshold (figures 7 (a) and (b)), at the end of the simulation. For both values of t_0 , the three curves are not far from overlapping with the time lag Δt normalized to a/c_s . This suggests a rather weak dependence on ρ_* of the correlation time, whatever the departure from the threshold and the magnitude of ρ_* . Such a scaling is expected when the correlation time scales like $\tau_c \approx a/c_s$. This is the case when the correlation is governed either by the parallel dynamics ($\tau_c \approx qR/v_{\parallel} \approx a/c_s$ at fixed aspect ratio R/a), or by the turbulence broadening ($\tau_c \approx \Delta\omega^{-1} \approx \omega_*^{-1} \propto a/c_s$ at $k_{\theta}\rho_i = \text{const}$). Though, the small mismatches observed in figure 6(a) for the case $\rho_* = 5.10^{-3}$ suggest that the correlation time weakly departs from this scaling at small ρ_* and far from the threshold. Since the correlation time seems to roughly scale like $\tau_c \approx a/c_s$, the Bohm or gyro-Bohm scalings would correspond to correlation lengths

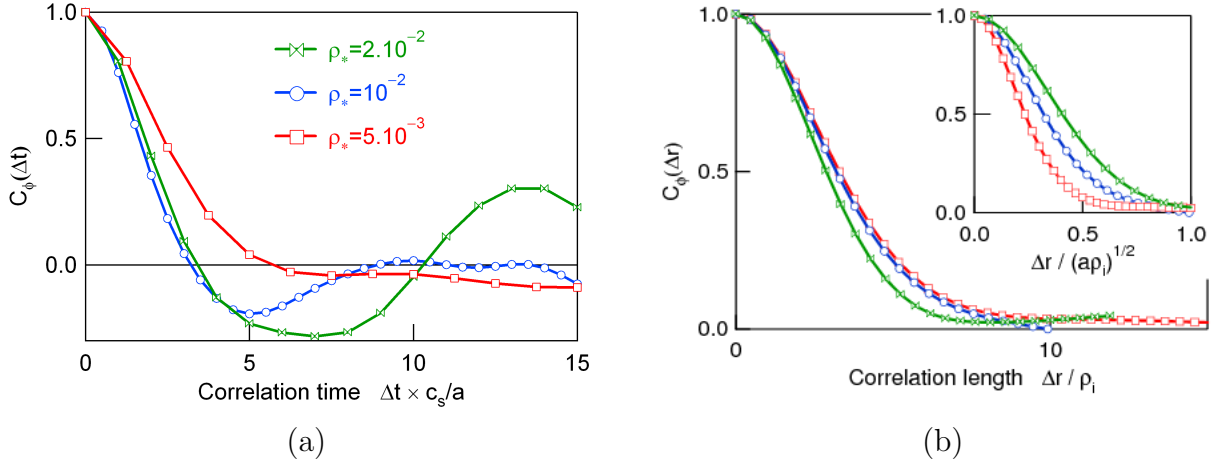


Figure 6. (Color online) (a) Temporal self-correlation function $C_{\delta\phi}(\Delta t)$ and (b) Radial self-correlation function $C_{\delta\phi}(\Delta r)$, for three values of ρ_* , well above the threshold.

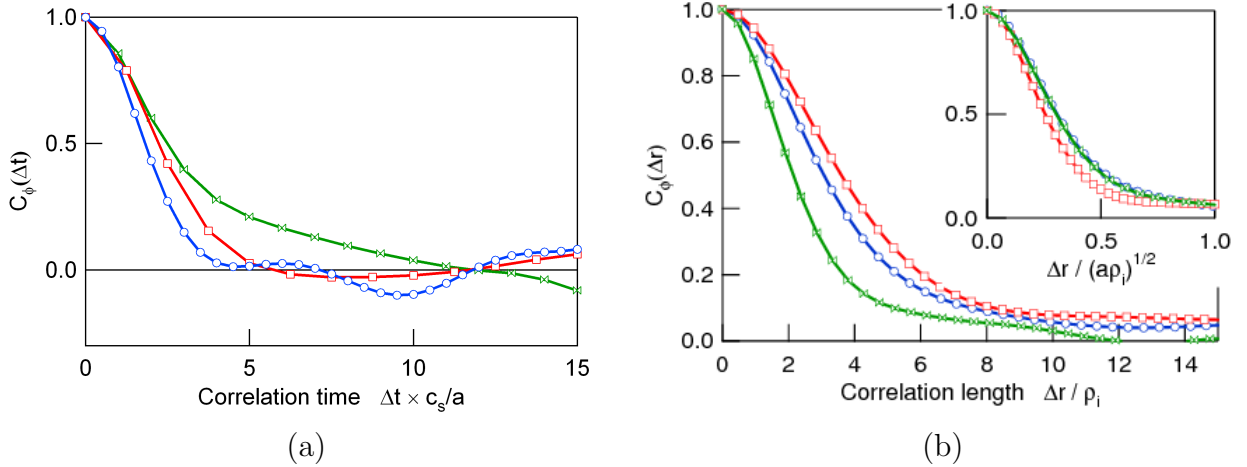


Figure 7. (Color online) (a) Temporal self-correlation function $C_{\delta\phi}(\Delta t)$ and (b) Radial self-correlation function $C_{\delta\phi}(\Delta r)$, for three values of ρ_* , close to the threshold.

of the order $\lambda_c \approx (a\rho_i)^{1/2}$ or $\lambda_c \approx \rho_i$, respectively. Such scalings are systematically checked for the two sets of analyzes, above (figure 6(b)) and close to (figure 7(b)) the threshold. The conclusions are as follows: λ_c scales like the ion Larmor radius ρ_i at small ρ_* and above the threshold, while it scales like $(a\rho_i)^{1/2}$ at large ρ_* and close to the threshold. Such a trend towards Bohm scaling would be expected when moving close to the threshold, due to possible long lived structures reminiscent of linear global modes.

In summary, it appears that the ρ_* scaling depends on both the distance to the threshold and on ρ_* . More precisely, Bohm-like scaling is observed close to the threshold and for large ρ_* , while gyro-Bohm scaling emerges above the threshold at small ρ_* . These results are consistent with previous publications. They put forward the need to go towards flux-driven simulations, so as to reach a statistical steady-state with a

well-defined mean temperature profile.

7. Flux driven gyrokinetics

Most present gyrokinetic simulations set the system out of equilibrium by imposing two thermal baths as radial boundary conditions. As shown here, such system then evolve leading to a relaxation of the gradients in the area of interest of the simulation domain. This evolution stops as the turbulence approaches the threshold where transport becomes very weak. In practice, during such a relaxation time, limited statistics are available to investigate the physics of scaling laws. An alternative approach is to maintain the system at prescribed gradients by prescribing ad'hoc sources to maintain them. In the latter case, it is an issue to determine the impact of such a fluctuating source on the turbulent transport properties. As achieved in standard fluid codes, a more physical drive can be obtained by prescribing a source term in the system that imposes a given flux and analyses the gradients as the response of flux driven turbulent transport. However, when going to gyrokinetic simulations this one to one relationship between a flux and a gradient is not as straightforward. Indeed, the gradients that are measured, say the temperature gradient, stem from a moment of the distribution function while the source term must be defined for each velocity of the distribution function and can thus generate gradients of higher moments of the distribution function.

First calculations of gyrokinetic flux driven systems [25] have been performed with a reduced gyrokinetic model that has been derived for deeply trapped ion turbulence [26, 9]. This system is 3D with two dimensions in real space, namely a radial coordinate and an angle and 1D in velocity space, the chosen coordinate being the energy. In such a system the source term is implemented at small radius (core heat source) in the vicinity of the core boundary layer where a vanishing gradient of the distribution function is imposed (symmetry conditions). To satisfy the boundary conditions a buffer zone with strong radial diffusion is imposed. In the simulations reported here, the source term is located at the boundary of the core buffer zone. Statistical equilibrium of such a system will of course not be satisfied unless one imposes a sink, typically at the radial edge boundary. We have chosen a prescribed temperature at this boundary condition, namely the distribution function is constrained to be a Maxwellian at fixed temperature T_{edge} . The large radial diffusion coefficient in the edge buffer region then allows the imposed heat flux to be transported through this boundary.

The choice of the source term must be as generic as possible, and with respect to our present scope, steady-state. In the present versions of our gyrokinetic codes, adiabatic electrons prevent particle transport so that the source term must not be a particle source. A simple approach has been followed by introducing the basis of Laguerre polynomials $L_n(E)$, where E is the energy normalized to T_{edge} and n the order of the polynomial (the exponent of the largest power in E). These Laguerre functions form an orthogonal basis where the scalar product is the integral over the energy E weighted by the Maxwellian $\exp(-E)$, see [9]. In such a framework, the projection of the distribution

function on the Laguerre polynomials, $G_k = \langle f | L_k \rangle$ (here $\langle f | g \rangle$ is the scalar product of f and g), is directly related to the fluid moments where the density is the projection on the zeroth order polynomial $L_0 = 1$ and the temperature $\sqrt{3/2}(T - T_{edge})/T_{edge}$ to the projection on $L_1 = \sqrt{2/3}(E - 3/2)$. For this reason the source term that has been used is $S = S_0(\psi) L_1(E) \exp(-E)$. Where $S_0(\psi)$ stands for the radial localisation labeled by ψ . By definition of such a source term, it only contributes to building up the moment $G_1 = \langle f | L_1 \rangle$ and thus governs an increase of the temperature at the source location. However, via the transport properties of the reduced Vlasov equation, such a moment is coupled to all the other moments [9]. The transport problem at hand is therefore the generation by the source of all G_k moments but G_0 towards the sink at the edge boundary where all moments G_k are vanishing but for $k = 0$. In practice, one finds that the time averaged moments (averaging over several confinement times) exhibit a flat profile between the very core and the source, and a smooth gradient from the source towards the vanishing values at the edge. Furthermore, one finds that the moment which exhibits the largest magnitude is the temperature moment, $k = 1$. The higher order moments with $k = 2$ to $k = 5$ are one order of magnitude smaller. The even higher moments $k > 5$ are negligible. Unlike the thermal bath boundary condition [9], one finds that a limited number of moments are active in the system with a possible truncation of the moment series at $k = 5$. However, such a property is related to the specific kinetic properties that have been selected for the source and sink. In particular, a less constrained sink allowing for a departure from a Maxwellian distribution function would modify the kinetic distortion of the distribution function. A final remark is related to the time averaged profiles that all appear to fit a diffusive transport process although the evolution of the system is characterized by strong relaxation events and the interaction between large $E \times B$ convection cells (extending over a significant fraction of the radial box size) and zonal flows [25].

8. Conclusion

Global and full- f 5D gyrokinetic codes are able to address additional pieces of crucial physics. Since they are facing new challenges in terms of numerical resources, they have only started being developed rather recently. The GYSELA code is one of those. The semi-Lagrangian numerical scheme, as well as an efficient parallelization, allow it to capture the dynamics of the whole ion distribution function in a simplified toroidal geometry. Linear and non-linear tests have been performed successfully. This paper reports a benchmark with the ORB5 code, modeling the same standard gyrokinetic equations for the Ion Turbulence Gradient driven turbulence with a completely different numerical scheme. Simulating a fraction of torus only reveals especially efficient in reducing the memory requirement and the CPU time consumption. This simplification is all the more valid since ρ_* is small. Three main physical issues have been discussed. First, the absence of scale separation assumption between the equilibrium and the fluctuations requires the former to be evaluated accurately. If not, large scale sheared flows

are shown to develop so as to counter-balance the curvature driven vertical charge polarization. Such sheared flows are observed to reducing the effective linear growth rate as well as delaying the onset of turbulence. Second, the scaling with ρ_* of the turbulent transport is investigated in a global geometry. Consistently with previous observations, the turbulence correlation properties are found to depend on ρ_* itself and on the distance to the threshold. The system exhibits a gyroBohm scaling well above the threshold at small values of ρ_* . Third, flux driven conditions can be addressed in such full- f codes, leading to statistical steady-state turbulent regimes. In this case, special emphasis is put on the departure of the distribution function from the Maxwellian in a reduced 3D model for interchange-like turbulence. It will be especially interesting to investigate how such complex kinetic characteristics extrapolate to the more realistic 5D ITG turbulent regime.

Acknowledgements: The authors wish to acknowledge the constant support of C. Passeron in the numerical development of the code. The strong commitment of M. Boulet (CEA/DAM), who has performed several runs on the Tera10 super-computer within the "Grand Challenge" project, is also warmly acknowledged.

- [1] Waltz R., Candy J., and Rosenbluth M. Gyrokinetic turbulence simulation of profile shear stabilization and broken gyrobohm scaling. *Phys. Plasmas*, 9(1938), 2002.
- [2] Lin Z., Chen L., and Zonca F. Role of nonlinear toroidal coupling in electron temperature gradient turbulence. *Phys. Plasmas*, 12:056125, 2005.
- [3] Jenko F., Dorland W., Kotschenreuther M., and Rogers B.N. Electron temperature gradient driven turbulence. *Phys. Plasmas*, 7(5):1904, 2000.
- [4] R. Hatzky S. Jolliet O. Sauter T. M. Tran L. Villard P. Angelino, A. Bottino. Effects of plasma current on nonlinear interactions of itg turbulence, zonal flows and geodesic acoustic modes. *Plasma Phys. Control. Fusion*, 48:557–571, 2006.
- [5] Grandgirard V. *et al.* A drift-kinetic semi-lagrangian 4d code for ion turbulence simulation. *Journal of Comput. Physics*, 217(2):395–423, 2006.
- [6] Grandgirard V. *et al.* Computing itg turbulence with a full- f semi-lagrangian code. *Comm. in Nonlinear Science and Numerical Simulation*, (doi:10.1016/j.cnsns.2007.05.016), 2007.
- [7] Dimits A. M. *et al.* Comparisons and physics basis of tokamak transport models and turbulence simulations. *Phys. Plasmas*, 7(3):969–983, 2000.
- [8] Bottino A., Tran T.M., Sauter O., Vaclavik J., and Villard L. Linear gyrokinetic simulations using particles for small perpendicular wavelength perturbations. *Th. Fusion Plasmas (Proc. Int. Workshop, Varenna, 2000)*, pages 327–332, 2001.
- [9] Sarazin Y., Grandgirard V., Fleurence E., Garbet X., and Ghendrih Ph. Kinetic features of interchange turbulence. *Plasma Phys. Control. Fusion*, 47, 2005.
- [10] Sonnendrucker E. and Roche J. The semi-lagrangian method for the numerical resolution of vlasov equation. *Journal of Comput. Physics*, 149:201–220, 1999.
- [11] Crouseilles N., Latu G., and Sonnendrucker E. Hermite splines interpolation on patches for a parallel solving of the vlasov-poisson equation. *Rapport INRIA RR5926*, 2006.
- [12] Latu G., Crouseilles N., Grandgirard V., and Sonnendrucker E. Gyrokinetic simulations in general geometry and applications to collisional damping of zonal flows. *submitted to PARSIM07*, 2007.
- [13] Idomura Y., Tokuda S., and Kishimoto Y. Global gyrokinetic simulation of ion temperature gradient driven turbulence in plasmas using a canonical maxwellian distribution. *Nuclear Fusion*, 43:234, 2003.

- [14] Angelino P., Bottino A., and Hatzky R. *et al.* On the definition of a kinetic equilibrium in global gyrokinetic simulations. *Phys. Plasmas*, 13:052304, 2006.
- [15] Dif-Pradalier G., Grandgirard V., and Sarazin Y. *et al.* Defining an equilibrium state in global full-f gyrokinetic models. *Communications in Nonlinear Science and Numerical Simulation*, page doi:10.1016/j.ensns.2007.os.004, 2007.
- [16] Garbet X., Sarazin Y., and Grandgirard V. *et al.* Beyond scale separation in gyrokinetic turbulence. *to appear in Nucl. Fusion*, 2007.
- [17] Dif-Pradalier G. *et al.* Gyrokinetic equilibrium and self-generated flows in tokamak plasmas. in preparation.
- [18] Rosenbluth M.N. and Hinton F.L. Poloidal flow driven by ion-temperature-gradient turbulence in tokamaks. *Phys. Rev. Letters*, 80(4), 1998.
- [19] Joliet S., Bottino A., and Hatzky R. *et al.* A global collisionless pic code in magnetic coordinates. *accepted for publication in Computer Physics Communications*, 2007.
- [20] Kadomtsev B.B. *Sov J. Plasma Phys.*, 1(295), 1975.
- [21] Ottaviani M., Beer M.A., Cowley S.C., Horton W., and Krommes J.A. *Phys. Rep.*, 283(121), 1997.
- [22] Lin Z., Ethier S., Hahm T.S., and Tang W.M. Size scaling of turbulent transport in magnetically confined plasmas. *Phys. Rev. Letter*, 88(195004), 2002.
- [23] Garbet X. and Waltz R. Action at distance and bohm scaling of turbulence in tokamaks. *Phys. Plasmas*, 3(1898), 1996.
- [24] Hahm T.S., Diamond P.H., Lin Z., Itoh K., and Itoh S-I. Turbulence spreading into the linearly stable zone and transport scaling. *Plasma Phys. Control. Fusion*, 46(A323), 2004.
- [25] Darmet G. *et al.* Intermittency in flux driven kinetic simulations of trapped ion turbulence. *Communications in Nonlinear Science and Numerical Simulation*, page doi:10.1016/j.cnsns.2007.05.024.
- [26] Depret G., Garbet X., Bertrand P., and Ghizzo A. Trapped-ion driven turbulence in tokamak plasmas. *Plasma Phys. Control. Fusion*, 23(42):949–971, 2000.